Supplementary Information

Differential microthermometry enables high-throughput calorimetry

Amin Kazemi, Mohammad Zargartalebi, David Sinton*

Department of Mechanical and Industrial Engineering, University of Toronto, 5 King's College Road, Toronto, Ontario, M5S 3G8, Canada.

*Correspondence and requests for materials should be addressed to David Sinton (E-mail: sinton@mie.utoronto.ca)

S1. Analysis of the existing continuous flow calorimeters

The principle of operation of currently available continuous flow calorimeters relies on measuring the power given to the flowing liquids. Here, we show the conditions that must be fulfilled during the operation of these instruments; otherwise, their results are disputable. A typical flow calorimeter is shown in Fig. S1. It consists of two stainless steel tubes with inner diameters typically a few hundred micrometers. Reference liquid and sample thermostated at T_{in} are injected in each tube at the same flowrate (Q). The heat fluxes q_r and q_s are given to the reference and the sample, respectively. The value of the sample heat flux is adjusted such that the temperatures at the outlet that the two thermistors show are equal (T_{out}). At this point, the relative specific heat capacity is calculated.

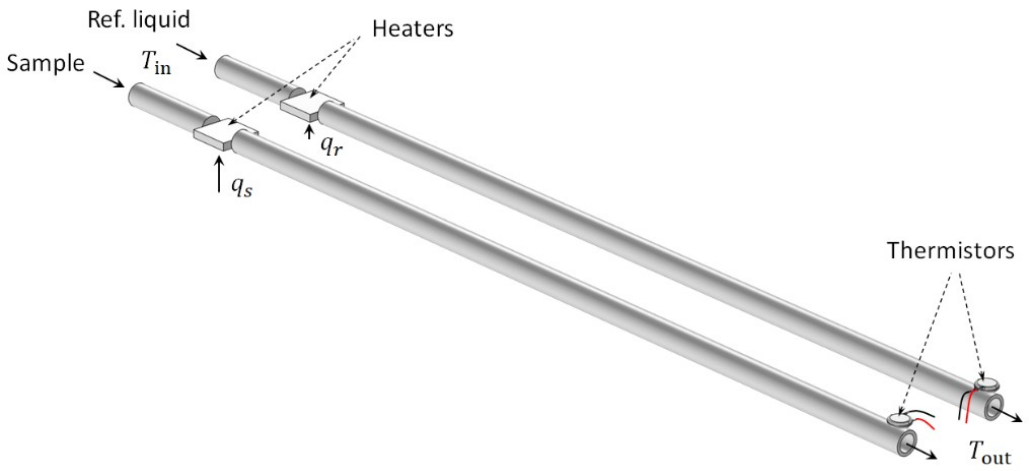

Fig. S1 A typical continuous flow calorimeter that works based on the measurement of heat fluxes. The heat flux given to the sample (q_s) is adjusted until the outlet temperature of both liquids (T_{out}) is equal.

Upon equality of the outlet temperatures, the energy balance for the reference liquid and the sample are given by:

$$q_r - q_{loss} = \rho Q C_p (T_{out} - T_{in}) \quad \text{(S1)}$$

and

$$q_s - q_{loss} = \rho' Q C_p' (T_{out} - T_{in}) \quad \text{(S2)}$$

where ρ and ρ' are the densities of the reference and sample, respectively, and q_{loss} is the total flux of heat loss (heat loss from the heaters to the ambient plus the heat that liquid loses as it flows in the tubes). The heat losses from both tubes are assumed to be equal when they have the same temperature distributions. The specific heat capacity of the sample is obtained by dividing eq(S2) by eq(S1):[1]

$$C_p' = C_p \left(\frac{\rho}{\rho'}\right)\left(\frac{q_s - q_{loss}}{q_r - q_{loss}}\right) \quad \text{(S3)}$$

In eq(S3), knowledge of heat loss is required to determine the specific heat capacity. Note that this problem also prevails in batch power-compensated calorimeters. In practice, a high vacuum is needed to minimize the heat loss and thus the measurement error. Even under a perfect vacuum, a fraction of the heat is lost through the radiation mechanism, being more pronounced at higher temperatures. Therefore, the results obtained by these calorimeters usually need to be corrected through an appropriate calibration procedure to account for the undesired heat loss. Accordingly, each instrument needs a specific calibration that should be performed under various operating conditions. The calibration factor may change from time

to time and is often unrepeatable. A comprehensive discussion on the effect of heat loss on this type of calorimeter may be found in reference [2] where it has been experimentally shown that at higher temperatures, this error could be as large as 40%.

A second approach would be to subtract eq(S1) from eq(S2) to eliminate the need to calculate the heat loss. In this case, the specific heat capacity after rearrangement is:

$$C_p^{'} = C_p\left(\frac{\rho}{\rho^{'}}\right) - \frac{q_r - q_s}{\rho^{'} Q\left(T_{out} - T_{in}\right)} \qquad \text{(S4)}$$

All terms in eq(S4) are measurable quantities, and one may determine $C_p^{'}$ through experimentations. The problem is that the determined $C_p^{'}$ is highly dependent on an accurate measurement of the individual heat fluxes q_r, q_s, and the temperature difference $\left(T_{out} - T_{in}\right)$. In fact, the measuring sensors need to be in direct contact with the liquids. More importantly, even if the sensors measure the actual temperatures, an ideal adiabatic condition for the fluid can not be expected, and the value of T_{out} is influenced by the conduction heat transfer along the tube walls (between T_{in} and T_{out}).[3] To diminish this effect, $\left(T_{out} - T_{in}\right)$ should be chosen as small as possible by giving infinitesimal heat fluxes to the liquids. However, this results in an increased temperature and heat flux measurement uncertainty due to low sensitivity. In the second approach, measurement of the absolute values of the heat fluxes is required, which is a major hurdle. Therefore, the operation of these calorimeters is restricted to a specific range which needs to be specified carefully. Otherwise, deviation of the results from the true values should be expected.

S2. Numerical simulation of the silicon chip calorimeter

The schematic representation of the chips and the dimensions are shown in Fig. S2. To investigate how much the thermal conductivities of the fluids affect the C_p measurements, we performed a numerical simulation of the system. The model solves the non-isothermal Navier Stokes equations in the liquid domains as well as the conduction heat transfer in the solids (both silicon and glass).

$$\nabla \cdot u = 0 \tag{S5}$$

$$\rho(u \cdot \nabla u) = \nabla \cdot \left[-PI + \mu\left(\nabla u + (\nabla u)^{tr}\right)\right] \tag{S6}$$

$$\rho u C_p \cdot \nabla T = \nabla \cdot (k \nabla T) \tag{S7}$$

where ***u*** is the velocity vector, ρ is the density, *P* is the pressure, ***I*** is the identity matrix, μ is the viscosity, *k* is the thermal conductivity, and C_p is the specific heat capacity at constant pressure. In the simulations, propylene glycol is used as the reference liquid and glycerol as the sample liquid. The liquids enter the channels from a small hole in the silicon wafer and exit from the other side. The temperature-dependent thermophysical properties of propylene glycol and glycerol are chosen as the default values in COMSOL (v5.6). The thermoelectric modules maintain the temperatures of the silicon chips at 40 °C on the hot side and 30 °C on the cold side. All other exposed areas can freely exchange heat with ambient ($T_\infty = 23\ ^\circ C$).

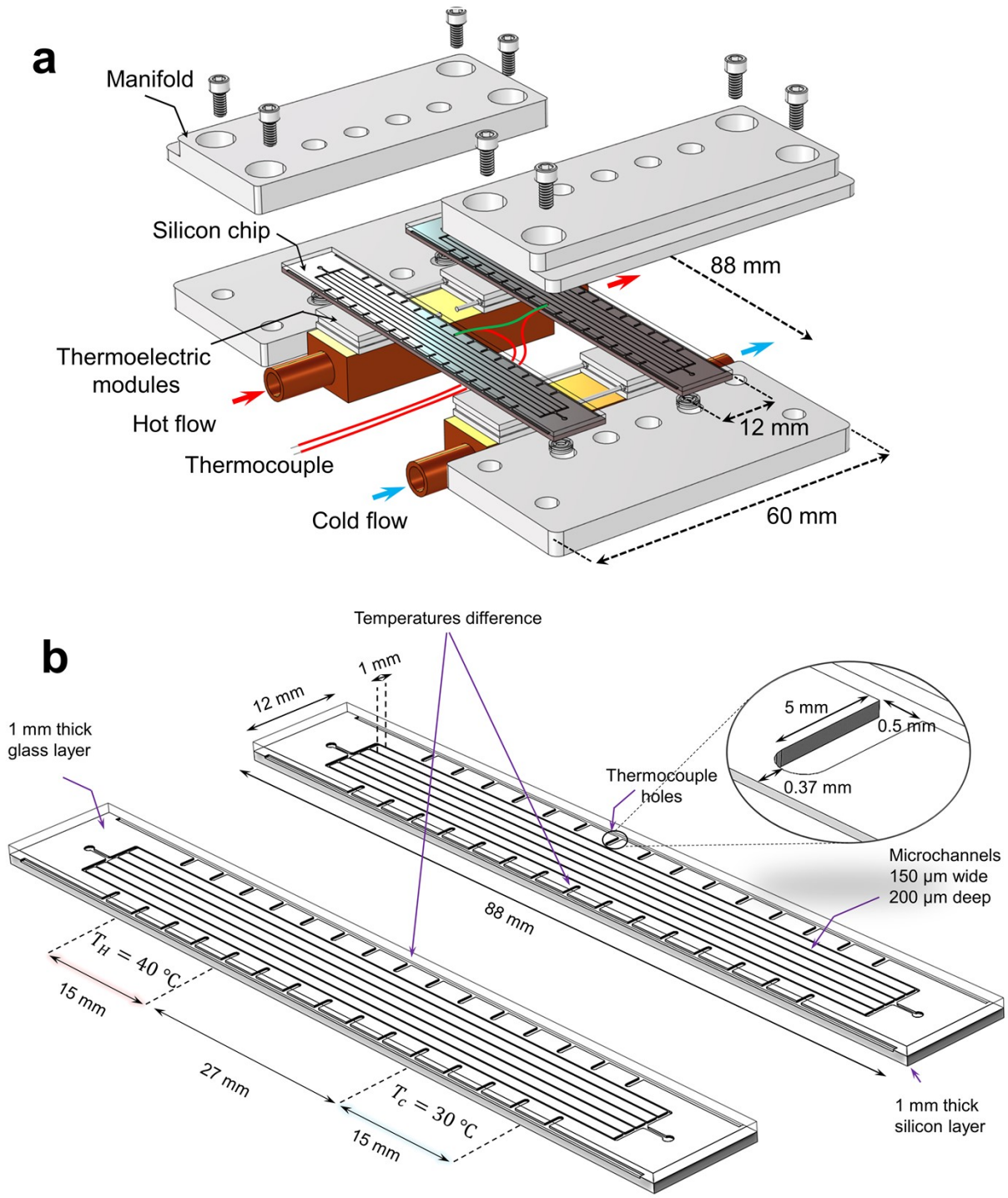

Fig. S2 Schematic representation of the microfluidic calorimeter and its dimensions. The colorimeter consists of a stainless-steel manifold to fix the silicon-glass chips in place and provide a sealed entrance and exit for fluids. Four thermoelectric modules are in contact with the copper blocks to enable a rapid change of T_h and T_c. b The depths of all etched patterns are 200 µm. The liquid inlets are on the silicon side at the bottom of the chips. The flow direction is from hot to cold.

The thermophysical properties of silicon wafer and borosilicate glass used in the simulations are summarized in Table S1. All temperatures are in Kelvin.

Table S1 Thermal properties of silicon wafer and glass used in the simulations.

Material	Physical property
Silicon wafer[¥]	$\rho\left[\frac{kg}{m^3}\right] = 2330$
	$k\left[\frac{W}{m\,K}\right] = -1.46\left(\frac{T}{298}\right)^3 + 18.31\left(\frac{T}{298}\right)^2 - 75.24\left(\frac{T}{298}\right) + 132.56$
	$C_p\left[\frac{J}{kg\,K}\right] = 65.87\left(\frac{T}{298}\right)^3 - 424.52\left(\frac{T}{298}\right)^2 + 953.90\left(\frac{T}{298}\right) + 117.31$
Borosilicate glass	$\rho\left[\frac{kg}{m^3}\right] = 2230$
	$k\left[\frac{W}{m\,K}\right] = 1.15$
	$C_p\left[\frac{J}{kg\,K}\right] = 800$

[¥]The correlations for the thermophysical properties of silicon wafer are obtained by fitting a cubic polynomial to the experimental data taken from:

https://analyzing-testing.netzsch.com/en/applications/photovoltaics/silicon-wafer-thermophysical-properties

In the simulations, the flowrate of the reference liquid (propylene glycol, C_p= 2568.8 J kg^{-1} K^{-1} and $\rho =$ 1034.8 kg m^{-3}) is set to Q = 0.04 mL/min, and that of the sample (glycerol) is adjusted to either 0.02 mL/min or 0.05 mL/min. By changing the sample flowrate from 0.02 to 0.05 mL/min, the differential thermocouple's reading changes from − 0.030 °C to 0.035 °C. Using linear interpolation, the sample flowrate that leads to a zero-temperature difference is Q' = 0.03393 mL/min. Thus, the specific heat capacity of glycerol is predicted to be:

$$C_p^{'} = C_p\left(\frac{\rho}{\rho^{'}}\right)\left(\frac{Q}{Q^{'}}\right) = 2568.8 \times \left(\frac{1034.8}{1262.1}\right) \times \left(\frac{0.04}{0.03393}\right) = 2482.9\frac{J}{kg \cdot K} \quad \text{(S8)}$$

where $Q^{'}$ is the sample flow rate. The densities are evaluated at 23°C. According to the COMSOL database, the specific heat capacity of glycerol at 35 °C is 2481.9 J kg^{-1} K^{-1}, and the proposed approach has an error of −0.04%, as suggested by the simulation results.

We also performed a numerical simulation of the flow calorimeter shown in section S1 using the same liquids and typical flowrates given in reference.[4] For that calorimeter, the heat flux ratio was adjusted until the average temperature of the liquids at the outlet matched. Based on the simulation results, considering an ideal condition of no heat loss from the device, the C_p of glycerol was predicted to be 1.5% higher than the established value. We further attempted to simulate the device by applying natural convection heat loss to the ambient. However, the liquid temperatures dropped progressively along the tubes, making the results length-dependent. As a result, the calorimeter is most likely not accurate if exchanging heat with the ambient.

S3. Measurement of enthalpy of phase change

In this section, we explore the potential to measure the enthalpy of phase change, such as using a 40% microencapsulated phase change material (PCM) slurry. This slurry primarily consists of n-paraffin waxes, such as nonadecane, encapsulated by a melamine resin membrane. For the numerical simulations, we utilized density, viscosity, thermal conductivity, and specific heat capacity values for the slurry from existing literature.[5] The viscosity of the 40% PCM slurry was estimated to be 225 times higher than that of its base fluid (water), as suggested in reference.[6]

The aim is to model the specific heat capacity (Cp) of the slurry and compare it with the Cp values obtained from differential scanning calorimetry (DSC). Details of the model may be found in section S2. We show that a differential microthermometry calorimetry approach can effectively capture the Cp gain resulting from phase change (Figure S3). This was achieved by stepwise increasing the temperature ($\Delta T = T_h - T_c = 2°C$), transitioning from below to above the material's melting temperature ($T_{melt} = 31$ ℃).

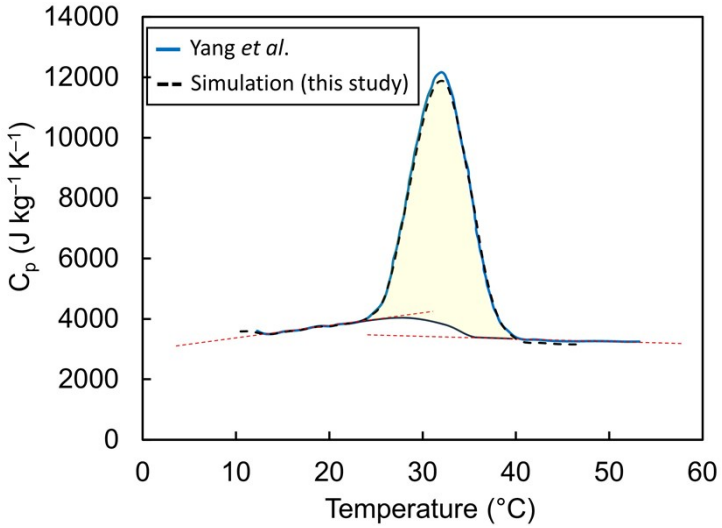

Fig. S3 Enthalpy of phase change. Specific heat capacity of 40% microencapsulated phase change slurry: Solid blue curve represents literature data,[6] dashed curve shows our simulation. The area under the curve denotes enthalpy of phase change, with a minor 0.5% deviation between DSC-measured latent heat (58.4 kJ/kg) and calculated one using the differential microthermometry approach (58.1 kJ/kg).

S4. Custom-built static mixer

To ensure efficient mixing in the studies with mixtures, a static mixer was fabricated and installed at the entrance of the sample chip. As shown in Fig. S4, the mixer includes alternating helical elements inserted in a plastic tube with an inner diameter of 500 µm. The helical elements were made by twisting the strips of aluminum foil and cutting them into small pieces. The lowest velocity in the tubes was 2.5 mm/s. At this velocity, the blue and yellow streams shown in 4c mixed well before entering the mixer, implying an efficient mixing of the liquids even in the absence of the mixer. To demonstrate the mixing ability of the mixer, the flowrates were increased until two distinct streams of yellow and blue liquids became visible before the mixer. A green liquid exiting the mixer was observed, indicating an acceptable mixing efficiency.

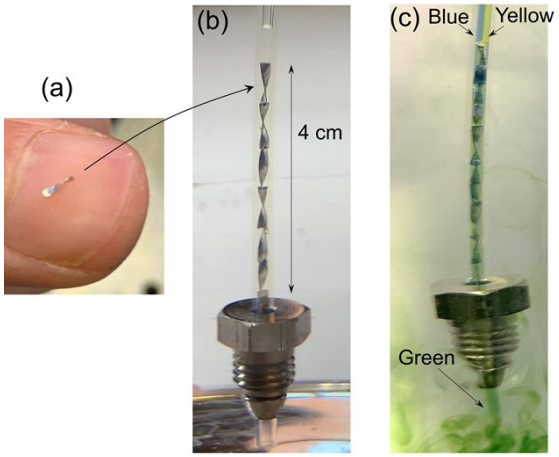

Fig. S4 Static mixer used for pre-mixing of the fluid streams. a mixer element on a human nail b image of the static mixer with six helical elements. c mixing a blue and yellow-dyed stream of water to test the mixing ability of the mixer. The flowrates were much higher than those used in the experiments. A Green stream at the outlet indicates good mixing efficiency. Note that the mixer is immersed in water, and the images are distorted.

S5. Effect of the Péclet number on the C_p measurement error

In Table S2, the measurement errors for different liquids at various Péclet numbers are listed. The data are sorted from large to small Péclet numbers. In the table, μ is the viscosity (Pa s), k is thermal conductivity (W m^{-1} K^{-1}), ρ is density (kg m^{-3}), $Q_{1/6}$ is the volumetric flow rate of the liquid in one of the six channels (mL/min), $C_{p,\,lit}$ and $C_{p,\,exp}$ are the literature and measured values of heat capacity (J kg^{-1} K^{-1}), respectively. *Re* is the Reynolds number, *Pr* is the Prandtl number, and *Pé* is the Péclet number. The error is calculated by 100× ($C_{p,\,exp}$–$C_{p,\,lit}$)/ $C_{p,\,lit}$.

Table S2 Error of the measurement at different Péclet numbers for various liquids

Compound	μ (Pa·s)	k (W/m K)	ρ (kg/m^3)	$Q_{1/6}$ (mL/min)	$C_{p,\,lit}$ (J/kg K)	$C_{p,exp}$ (J/kg K)	*Re*	*Pr*	*Pé*	Error %
n-Decane	0.000709	0.13	719.2	0.02534	2246.1	2254.4	3.18	12.18	38.76	0.37
Heptane	0.000386	0.12	671.3	0.02263	2282.7	2247.3	4.87	7.26	35.35	−1.55
Hexane	0.000291	0.12	645.7	0.02256	2302.7	2339.3	6.20	5.59	34.62	1.59
Octane	0.000456	0.13	691.2	0.02194	2261.9	2254.3	4.12	8.18	33.72	−0.33
Undecane	0.000942	0.14	729.3	0.02149	2242.9	2185.7	2.06	15.16	31.25	−2.55
Dodecane	0.001156	0.14	738.1	0.02088	2236.4	2223.7	1.65	18.80	31.04	−0.57
Butyl acetate	0.000585	0.13	831.8	0.02030	1948.9	1948.8	3.58	8.58	30.68	0.00

Compound	μ (Pa·s)	k (W/m K)	ρ (kg/m³)	$Q_{1/6}$ (mL/min)	$C_{p,\ lit}$ (J/kg K)	$C_{p,exp}$ (J/kg K)	*Re*	*Pr*	*Pé*	Error %
Ethylene glycol	0.011880	0.17	1103.1	0.01522	2458.2	2462.3	0.17	168.81	29.54	0.17
Hexane	0.000291	0.12	645.7	0.01904	2302.7	2257.9	5.23	5.59	29.21	−1.95
Butanol	0.001992	0.15	798.0	0.01757	2490.8	2462.6	0.87	33.08	28.84	−1.13
Heptane	0.000386	0.12	671.3	0.01837	2282.7	2215.5	3.95	7.26	28.69	−2.94
Propanol	0.001540	0.15	791.8	0.01753	2497.7	2466.4	1.12	25.14	28.07	−1.25
Octane	0.000456	0.13	691.2	0.01798	2261.9	2200.7	3.38	8.18	27.63	−2.70
Ethanol	0.000895	0.16	776.7	0.01740	2526.3	2531.1	1.87	13.87	25.95	0.19
EG	0.011880	0.17	1103.1	0.01296	2458.2	2406.6	0.15	168.81	25.16	−2.10
Undecane	0.000942	0.14	729.3	0.01701	2242.9	2212.2	1.63	15.16	24.74	−1.37
Dodecane	0.001156	0.14	738.1	0.01627	2236.4	2282.2	1.29	18.80	24.20	2.05
Hexadecane	0.002480	0.14	763.1	0.01589	2238.3	2268.1	0.61	39.96	24.19	1.33
Butyl acetate	0.000585	0.13	831.8	0.01581	1948.9	2001.2	2.79	8.58	23.90	2.68
Propanol	0.001540	0.15	791.8	0.01429	2497.7	2441.1	0.91	25.14	22.88	−2.27
Butanol	0.001992	0.15	798.0	0.01357	2490.8	2550.0	0.67	33.08	22.27	2.38
Acetone	0.000282	0.16	774.6	0.01582	2191.6	2224.6	5.38	3.94	21.18	1.51
Ethanol	0.000895	0.16	776.7	0.01395	2526.3	2526.3	1.50	13.87	20.80	0.00
Ethanol	0.000895	0.16	776.7	0.01388	2526.3	2538.1	1.49	13.87	20.70	0.47
PG	0.042000	0.22	1027.6	0.01354	2566.1	2577.0	0.04	499.66	20.50	0.43
EG	0.011880	0.17	1103.1	0.01038	2458.2	2404.5	0.12	168.81	20.14	−2.18
Ethanol	0.000895	0.16	776.7	0.01330	2526.3	2588.9	1.43	13.87	19.83	2.48
PG	0.042000	0.22	1027.6	0.01090	2566.1	2579.3	0.03	499.66	16.50	0.51
Ethanol	0.000895	0.16	776.7	0.01100	2526.3	2469.5	1.18	13.87	16.40	−2.25
Glycerol	0.934000	0.29	1260.0	0.01170	2400	2352.6	0.00	7676.71	15.00	−1.97
Formamide	0.003230	0.35	1120.3	0.01302	2413.9	2354.9	0.56	22.10	12.36	−2.45
Glycerol	0.934000	0.29	1260.0	0.00922	2400	2393.2	0.00	7676.71	11.82	−0.28
PG	0.042000	0.22	1027.6	0.00700	2566.1	2537.3	0.02	499.66	10.60	−1.12
Formamide	0.003230	0.35	1120.3	0.01016	2413.9	2348.2	0.44	22.10	9.65	−2.72
Water	0.000720	0.60	991.4	0.01000	4178.2	4181.6	1.71	5.03	8.58	0.08
Water	0.000720	0.60	991.4	0.00833	4178.2	4169.2	1.42	5.03	7.15	−0.22
Water	0.000720	0.60	991.4	0.00667	4178.2	4173.3	1.14	5.03	5.72	−0.12
Ethanol	0.000895	0.16	776.7	0.00382	2526.3	2307.9	0.41	13.87	5.69	−8.64
Ethanol	0.000895	0.16	776.7	0.00194	2526.3	2275.6	0.21	13.87	2.89	−9.92
Water	0.000720	0.60	991.4	0.00333	4178.2	4181.6	0.57	5.03	2.86	12.44
Water	0.000720	0.60	991.4	0.00167	4178.2	4181.6	0.28	5.03	1.43	7.97
Water	0.000720	0.60	991.4	0.00083	4178.2	4181.6	0.14	5.03	0.71	−4.63
Water	0.000720	0.60	991.4	0.00017	4178.2	4181.6	0.03	5.03	0.14	16.45

S6. Influence of the liquid thermal conductivity on the measured C_p

Devising a definitive experiment to isolate thermal conductivity from other properties would be unattainable. For example, nanofluids could be added to enhance the thermal conductivity of a liquid, but other physical properties, such as specific heat capacity and density, would change accordingly. We used numerical simulations to determine how much the thermal conductivities affect the C_p measurements. For this purpose, we artificially multiplied the thermal conductivity of the reference liquid (propylene glycol) by ten and repeated the simulations that were explained in section S2. As a result of this change, the predicted heat capacity of the sample liquid (glycerol) changed from 2483.2 to 2481.8 J kg^{-1} K^{-1}. Thus, by increasing the thermal conductivity by 1000%, the predicted heat capacity showed a −0.06% change. We further investigated the effect of thermal conductivities by reducing the thermal conductivity of propylene glycol by 10-fold and obtained a heat capacity of 2488.04 J kg^{-1} K^{-1} for glycerol. This corresponds to a 0.2% error in the predicted C_p. The analysis, therefore, confirms the independence of the proposed approach to the liquid thermal conductivities at typical operating conditions used in the experiments. The same procedure was repeated for the tube calorimeter shown in section S1. The analysis showed that increasing the thermal conductivity of propylene glycol by ten times changes the predicted C_p by 0.07%. However, a ten-time decrease in thermal conductivity increased C_p by 3.5%, which is not negligible. This effect was 0.2% for our chip calorimeter, indicating the independence of our approach to liquid thermal conductivity.

S7. Switching the sample and reference channels

Here, we show that the chips are interchangeable, meaning that the selection of the chip for the reference liquid and the sample is inconsequential. To assess chip-to-chip reproducibility, we measured the specific heat capacities of five liquids at 25 °C. A list of the liquids and their measured heat capacities are provided in Table S3. The results are the average of three experiments. A comparison between the C_p measured in chip 1 and those measured in chip 2 is shown by a parity plot in Fig. S5. A correlation coefficient of R^2=0.99998 was found between the heat capacities in chip 1 and chip 2, indicating a negligible difference. This finding is visually represented in Fig. S5. where the error bars, representing the standard deviations of the measurements, align closely with the 45° line, further reinforcing the convergence of the data points.

Table S3 Specific heat capacities of five liquids (J/kg K) measured at 25 °C using either chip.

	Sample in chip 1					Sample in chip 2				
Compound	Run 1	Run 2	Run 3	Average	std	Run 1	Run 2	Run 3	Average	std
Dodecane	2234.2	2209.4	2241.7	2228.4	13.8	2197.6	2232.8	2227.1	2219.2	15.4
Ethanol	2469.3	2442.7	2450.0	2454.0	11.2	2429.5	2452.6	2459.9	2447.3	13.0
Formamide	2352.4	2367.2	2401.4	2373.7	20.5	2342.1	2364.9	2366.6	2357.9	11.2
Glycerol	2342.5	2329.1	2353.7	2341.8	10.1	2355.4	2338.9	2366.7	2353.7	11.4
Heptane	2238.2	2224.8	2259.2	2240.7	14.2	2229.7	2258.3	2242.8	2243.6	11.7

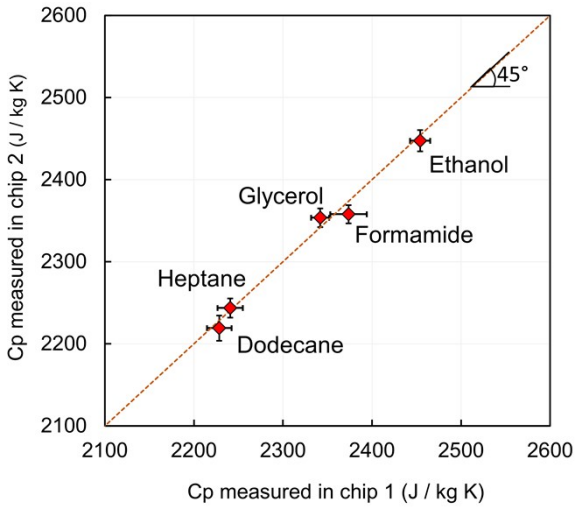

Fig. S5 Parity plot showing the specific heat capacities measured in chip 2 vs. those measured in chip 1. Error bars are standard deviations which may be found in Table S3.The correlation coefficient of a fitted line to the data with a zero intercept is found to be R^2=0.99998.

S8. Effect of heat loss

The effect of heat loss on the C_p measurements is investigated both experimentally and theoretically. For the experiments, we insulated the microfluidic chip using a layer of polyamide tape followed by a layer of foam insulation tape (~5 mm thick). For a typical experiment with water (reference fluid) and glycerol (sample) at 60 °C (T_h= 70 °C and T_c= 50 °C), the measured heat capacities are listed in Table S4. Each experiment was performed three times, and the results were averaged. The investigation showed that the insulation of the chip did not make any significant change in the measured C_p. When insulated, the device yielded C_p= 2529.6 ± 8.8 J kg^{-1} K^{-1} showing a −1.0 % error as compared to the literature value. However, when insulations are removed, it measured C_p = 2546.3 ± 11.8 J kg^{-1} K^{-1}, showing a −0.4% error with the literature value. Note that considering the standard deviations, both measurements overlap; therefore, no measurable difference could be identified.

Table S4 Experimental C_p of glycerol measured with and without insulating the chips.

	Run 1	Run 2	Run 3	Average ± std	Error (%) with the literature value
C_p with insulation (J kg^{-1} K^{-1})	2527.7	2541.3	2519.9	2529.6 ± 8.8	−1.0 %
C_p without insulation (J kg^{-1} K^{-1})	2539.6	2572.9	2544.5	2546.3 ± 11.8	−0.4 %

We also investigated the effect of heat loss numerically. In the simulations, the heat transfer coefficient between the chip and the ambient air (T_∞ = 23 °C) was set to different values of 0, 1, 10, 100, 1000, and 10000 Wm^{-2} K$^{-1,}$ and C_p of glycerol was predicted. The numerical results suggested that the change in the predicted C_p compared to the case of no heat loss does not exceed 1.2%, as shown in Fig. S6. Typical heat transfer coefficients for free convection of air fall within 2.5–25 Wm^{-2} K^{-1} (chapter 14 of reference [7]). Thus, based on Fig. S6, the deviation of C_p from the case of zero heat loss should be negligible.

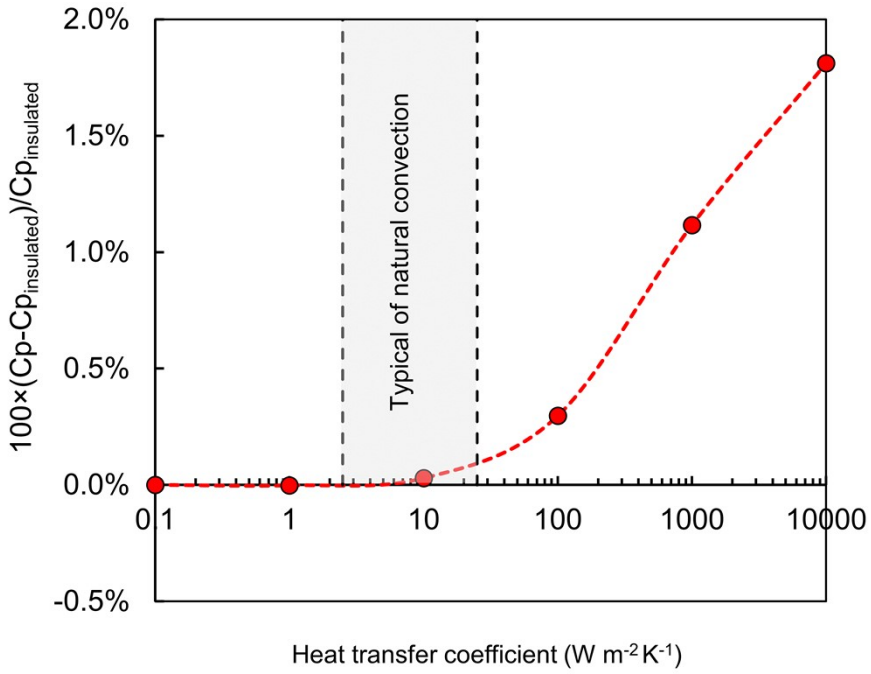

Fig. S6 Deviation of the simulated heat capacity of glycerol from the ideal case of zero heat loss. The horizontal axis is the heat transfer coefficient between the chip and the ambient.

Reference

1. Rogers, P. S. Z. & Sandarusi, J. A completely automated flow, heat-capacity, calorimeter for use at high temperatures and pressures. *Review of Scientific Instruments* **61**, 3440 (1998).

2. White, D. E. & Wood, R. H. Absolute calibration of flow calorimeters used for measuring differences in heat capacities. A chemical standard for temperatures between 325 and 600K. *Journal of Solution Chemistry 1982 11:4* **11**, 223–236 (1982).

3. Höhne, G. W. H., Hemminger, W. F. & Flammersheim, H.-J. *Differential Scanning Calorimetry*. (Springer Berlin Heidelberg, 2003).

4. Picker, P., Leduc, P. A., Philip, P. R. & Desnoyers, J. E. Heat capacity of solutions by flow microcalorimetry. *J Chem Thermodyn* **3**, 631–642 (1971).

5. Zhang, Y., Wang, S., Rao, Z. & Xie, J. Experiment on heat storage characteristic of microencapsulated phase change material slurry. *Solar Energy Materials and Solar Cells* **95**, 2726–2733 (2011).

6. Yang, R., Xu, H. & Zhang, Y. Preparation, physical property and thermal physical property of phase change microcapsule slurry and phase change emulsion. *Solar Energy Materials and Solar Cells* **80**, 405–416 (2003).

7. Kosky, P., Balmer, R., Keat, W. & Wise, G. Mechanical Engineering. *Exploring Engineering* 259–281 (2013) doi:10.1016/B978-0-12-415891-7.00012-1.